JACS
JOURNAL OF THE AMERICAN CHEMICAL SOCIETY
Article
pubs.acs.org/JACS

Adaptive Accelerated ReaxFF Reactive Dynamics with Validation from Simulating Hydrogen Combustion

Tao Cheng,[†,‡] Andrés Jaramillo-Botero,*[,‡] William A Goddard, III,*[,‡] and Huai Sun*[,†]

[†]School of Chemistry and Chemical Engineering, Shanghai Jiao Tong University, Shanghai 200240, China
[‡]Materials and Process Simulation Center, California Institute of Technology, Pasadena, California 91125, United States

Supporting Information

ABSTRACT: We develop here the methodology for dramatically accelerating the ReaxFF reactive force field based reactive molecular dynamics (RMD) simulations through use of the bond boost concept (BB), which we validate here for describing hydrogen combustion. The bond order, undercoordination, and overcoordination concepts of ReaxFF ensure that the BB correctly adapts to the instantaneous configurations in the reactive system to automatically identify the reactions appropriate to receive the bond boost. We refer to this as adaptive Accelerated ReaxFF Reactive Dynamics or aARRDyn. To validate the aARRDyn methodology, we determined the detailed sequence of reactions for hydrogen combustion with and without the BB. We validate that the kinetics and reaction mechanisms (that is the detailed sequences of reactive intermediates and their subsequent transformation to others) for H_2 oxidation obtained from aARRDyn agrees well with the brute force reactive molecular dynamics (BF-RMD) at 2498 K. Using aARRDyn, we then extend our simulations to the whole range of combustion temperatures from ignition (798 K) to flame temperature (2998K), and demonstrate that, over this full temperature range, the reaction rates predicted by aARRDyn agree well with the BF-RMD values, extrapolated to lower temperatures. For the aARRDyn simulation at 798 K we find that the time period for half the H_2 to form H_2O product is ~538 s, whereas the computational cost was just 1289 ps, a speed increase of ~0.42 trillion (10^{12}) over BF-RMD. In carrying out these RMD simulations we found that the ReaxFF-COH2008 version of the ReaxFF force field was not accurate for such intermediates as H_3O. Consequently we reoptimized the fit to a quantum mechanics (QM) level, leading to the ReaxFF−OH2014 force field that was used in the simulations.

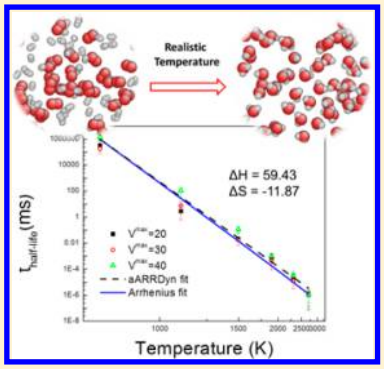

1. INTRODUCTION

Most chemical processes involve a complex system of interacting molecules and atoms in which collisions can energize molecules sufficiently to break existing bonds and form new ones. Determining the reaction mechanisms, that is the sequences of reaction steps and product distributions and how they depend on temperature, pressure, and concentrations is very difficult because of multiple collisions of energized molecules. The exception is the case of very dilute low-pressure low temperature reactions, where bimolecular and unimolecular processes dominate the reactive events. In such cases, an excellent understanding of the details for many processes has been obtained by combining theory and experiment to provide an exquisite description of even subtle processes involving coupling of vibrational, rotational, and electronic excitations.[1] Our goal is to extend this level of mechanistic understanding to high pressure, high temperature, nonequilibrium systems relevant for such chemical processes as chemical vapor deposition (CVD), atomic layer deposition (ALD), shock induced decompositions and reactions, combustion, and propulsion. We report here what we consider to be a dramatic step forward in accomplishing this.

The problem with molecular dynamics (MD) simulations of reactions is that most of the time the atoms are vibrating and bouncing around with no reactions, then very occasionally part of the system is sufficiently energized that a reactive step occurs. Following the RMD for a billion dynamics steps using a 1 fs time step (a microsecond) to finally observe each rare reaction event is impractical. To tackle this rare-event problem, transition state focused methods of accelerated dynamics have been developed to identify transition pathways between known initial and final states. Example implementations include targeted molecular dynamics,[2] transition path sampling,[3] and essential molecular dynamics.[4] However, these approaches assume that the reaction steps are already known. In contrast hyperdynamics techniques explore the potential energy surfaces (PES) without requiring prior knowledge of reaction pathways, by efficiently identifying regions of phase space that dominate the reaction steps. These hyperdynamics methods include replica exchange MD[5,6] metadynamics,[7] hyperdynamics,[8,9] temperature accelerated dynamics,[10,11] kappa dynamics,[12] bond boost (BB),[13−20] and accelerated molecular dynamics (AMD) methods.[21−36]

Hyperdynamics methods[8,9] can produce information on both kinetics and thermodynamics, but calculations to determine transition states are too demanding. The BB variation[13,14] of hyperdynamics employs simple rules based on bond lengths to

Received: April 14, 2014
Published: June 2, 2014

   dx.doi.org/10.1021/ja5037258 | J. Am. Chem. Soc. 2014, 136, 9434−9442

identify the transition state and then applies a boost potential based on these bond lengths. This decreases computational costs, making it applicable to realistic systems. Successful results using BB have been reported on surface diffusion,[14] desorption,[17] and film growth.[18] Although the concepts of accelerated dynamics developed over the past decade have been applied to a number of hyperdynamics processes, these techniques have not yet been applied to realistic chemical reaction processes.

We describe here how to combine Reactive Molecular Dynamics (RMD) based on the ReaxFF reactive force field with accelerated dynamics concepts to simulate long-term realistic chemical reaction processes. Our formulation is patterned after the bond boost (BB) method developed to work with classical force fields, but modified to use the bond order concepts present in ReaxFF. We refer to this approach as adaptive Accelerated ReaxFF Reaction Dynamics or aARRDyn.

To validate the aARRDyn methodology we consider the combustion of H_2/O_2 mixtures. In this case, it is well-known that there are just a few important intermediates (HO_2, H, HO, O), with only two stable initial products (HOH and HOOH). Despite the simplicity, BF-RMD takes too long in real time to convert the reactants all the way to HOH at, say, the ignition temperatures, requiring the RMD to be done at high temperature. For example, at the ignition temperature for H_2 oxidation (798 K), we estimate that it takes 1000 s for half the H_2 to form H_2O product based on an Arrhenius fit from the calculated reaction barrier from BF-RMD, which would require ~4 quintillion (10^{18}) times steps for BF-RMD. Doing this 4 quintillion (10^{18}) time steps for good statistics, makes the BF-RMD approach quite impractical. In contrast, we find that with aARRDyn, this will reduce to ~4000 thousand time steps, for which the computational cost is equivalent to 1000 ps of BF-RMD, a speed up by a factor of 1 trillion (10^{12}).

To validate aARRDyn against BF-RMD, we carried out BF-RMD at a sufficiently high temperature, 2498 K for H_2 oxidation for 19 independent ReaxFF simulations (requiring ~10 ns each) to follow the production of intermediates and products. Then we validate that the aARRDyn (again for 19 cases) dramatically decreases the simulation time while producing the same sequence of reaction intermediates and the same kinetics parameters (after converting the times in aARRDyn from MD time to hypertime).

In addition to validating aARRDyn, reactions involving the combustion of H_2 at higher pressures and lower temperatures have not been fully elucidated, making the detailed study of mechanistic steps very important. The combustion of H_2 is exoergic, making H_2 one of the highest energy fuels for rocket science and transportation (new generation fuel cells).[37] Also, H_2 is a green energy resource, since it does not produce unwanted emissions during combustion. Yet, in order to improve the design of combustion system for hydrogen, details on the mechanism of H_2 combustion under high pressure, low temperature, and nonequilibrium conditions need further elucidation. Here, ReaxFF-based RMD allows one to simulate the combustion mechanisms at atomic scales.[38−41] Previously, no such realistic combustion simulations at realistic temperatures have been reported, because BF-RMD simulations cannot yet reach the millisecond time scale needed to directly simulate the combustion reactions at the most interesting temperatures.

In this paper we outline the implementation of the aARRDyn method into the ReaxFF/PuReMD software suite[42] and we compare the results of simulating hydrogen combustion using aARRDyn to standard BF-RMD to provide validation. We benchmark the reaction kinetics and reaction mechanisms from aARRDyn against BF-RMD using exactly the same ReaxFF field for 19 independent simulations to increase the statistical accuracy of our comparisons (Supporting Information, Figure S1 shows one case of the statistics). Furthermore, we demonstrate the validity of aARRDyn over the broad temperature range of H_2 combustion temperatures, from ignition (798 K) to flaming (2998 K).

In carrying out these RMD simulations we found that the ReaxFF-COH2008 version of the ReaxFF force field was not accurate for such intermediates as H_3O. Consequently we reoptimized the fit from quantum mechanics (QM) results at the level of B3LYP/6-311G**, leading to the ReaxFF-OH2014 force field that was used in the simulations, and which is reported in the Supporting Information.

2. THEORY AND METHOD

2.1. Theory. In the original BB method,[13,14] the tagged bonds depend solely on the bond length. This is a good approximation for dynamics of nonreactive systems, but for chemically reacting system, it is not sufficiently accurate. Here, the connectivity between atoms depends not just on the pairwise distance, but also on the valence and bonding states of the atoms involved. To address this issue we use the ReaxFF reactive force field framework to provide the essential information. Thus, at each step of the dynamics we use the bond order (BO) concept of ReaxFF to identify bonds weak enough to be approaching a transition state, but we refrain from selecting species whose bond may have already broken (radicals) so as to not interfere with their dynamics which might select between various intermediate or product states.

As described below aARRDyn uses concepts of bond order, overcoordination, and undercoordination that are already calculated as part of the ReaxFF force evaluations, so that aARRDyn does not introduce new computational overhead, making its introduction into ReaxFF RMD framework simple and efficient.

In ReaxFF, the bond order expression contains contributions from sigma, pi, and double pi type bonds, with the form:

$$\begin{aligned} BO'_{ij} &= BO^{\sigma}_{ij} + BO^{\pi}_{ij} + BO^{\pi\pi}_{ij} \\ &= \exp\left[p_{bo1}\left(\frac{r_{ij}}{r_0^{\sigma}}\right)^{p_{bo2}}\right] + \exp\left[p_{bo3}\left(\frac{r_{ij}}{r_0^{\pi}}\right)^{p_{bo4}}\right] \\ &\quad + \exp\left[p_{bo5}\left(\frac{r_{ij}}{r_0^{\pi\pi}}\right)^{p_{bo6}}\right] \end{aligned} \tag{1}$$

Given the bond orders of an atom to all its neighbors, ReaxFF then makes corrections based on whether the sum of bond orders is larger than the valence of the atom (overcoordinated) or smaller than the valence (undercoordinated).The uncorrected overcoordination, Δ_i', was originally defined as the difference between the total bond order around an atom and the number of its bonding electrons (Val_i),

$$\Delta' = -Val_i + \sum_{j=1}^{\text{neighbors}(i)} BO'_{ij} \tag{2}$$

but was later modified by a second order coordination term, $\Delta_i'^{boc}$ to soften the correction for atoms bearing lone electron pairs,

$$\Delta_i'^{boc} = -Val_i^{boc} + \sum_{j=1}^{\text{neighbors}(i)} BO'_{ij} \tag{3}$$

as described by Chenoweth et al.[39] (reproduced here in the Supporting Information). A corrected over coordination is then

dx.doi.org/10.1021/ja5037258 | J. Am. Chem. Soc. 2014, 136, 9434−9442

derived from the corrected bond orders, which are in turn used to calculate the dependence of the bond energies on distance,

$$E_{\text{bond}} = -D_e^{\sigma}\text{BO}_{ij}^{\sigma}\exp[p_{\text{be1}}(1-(\text{BO}_{ij}^{\sigma})^{p_{\text{be2}}})] - D_e^{\pi}BO_{ij}^{\pi} - D_e^{\pi\pi}D_{ij}^{\pi\pi} \quad (4)$$

The corrected bond orders are critical to obtain accurate condensed phase properties, because bonded atoms and nonbonded neighbor atoms may have similar interaction distances. In this work, we use $\text{BO}_{\text{cut}} = 0.3$ to determine the bonds to tag for a bond boost.

The original BB method has been described in detail elsewhere.[13,14] The basic concept behind BB is simply to introduce a boost potential that reduces the time to overcome potential barriers. The boost potential is expressed as a function of bond lengths, and given by

$$\Delta V\{x_1, x_2...x_N\} \equiv \Delta V\{r_1, r_2...r_{N_b}\} \quad (5)$$

where, N is the total number of atoms, N_b is the total number of bonds in the simulation system, and r_i is the length of each bond. Furthermore, a fractional change (ε_i) in bond length from the equilibrium bond length (r_i^{eq}) is defined as follows:

$$\varepsilon_i = \frac{r_i - r_i^{\text{eq}}}{r_i^{\text{eq}}} \quad (6)$$

Then, the boost potential becomes a function of bond fractional changes, ε_i, as

$$\Delta V\{x_1, x_2...x_N\} \equiv \Delta V\{\varepsilon_1, \varepsilon_2...\varepsilon_{N_b}\} \quad (7)$$

An empirical threshold parameter, q, was defined to ensure that the boost energy is not applied to transition states. In this paper we apply BB only when both BO > BOcut = 0.3 and $\varepsilon_i < q = 0.5$.

The boost potential, ΔV, consists of an "envelope function", and a boost potential applied to each bond, $\delta V(\varepsilon_i)$, as follows:

$$\Delta V\{\varepsilon_1, \varepsilon_2...\varepsilon_{N_b}\} = A\{\varepsilon_1, \varepsilon_2...\varepsilon_{N_b}\}\sum_{i=1}^{N_b}\delta V(\varepsilon_i) \quad (8)$$

The boost potential applied to each bond is defined as follows:

$$\delta V\{\varepsilon_i\} = \frac{\Delta V^{\max}}{N_b}\left[1-\left(\frac{\varepsilon_i}{q}\right)^2\right] \quad (9)$$

where $\Delta V^{\max}$ controls the amplitude of the boost potential. The idea of an "envelope function", $A\{\varepsilon_1, \varepsilon_2, ..., \varepsilon_{\text{Nb}}\}$, is to channel energy into the bond that is closest to reacting. The bond change is determined by ε_i. The bond with the largest ε ($\varepsilon^{\max}$) is considered to be the one closest to breaking. The envelope function is defined as

$$A\{\varepsilon_1, \varepsilon_2...\varepsilon_{N_b}\} = A\{\varepsilon^{\max}\} = \left[1-\left(\frac{\varepsilon^{\max}}{q}\right)^2\right]\frac{1-(\varepsilon^{\max}/q)^2}{1-P_1^2\left(\frac{\varepsilon^{\max}}{q}\right)^2} \quad (10)$$

Here, P_1 is a parameter to control the curvature near the boundary. The effect of the envelope function is clearer from the force calculation:

$$\delta F_i = -\frac{\mathrm{d}}{\mathrm{d}r_i}\Delta V = \begin{cases} -A(\varepsilon^{\max})\dfrac{\mathrm{d}}{\mathrm{d}r_i}\delta V(\varepsilon_i), & \text{if } \varepsilon_i < \varepsilon^{\max} \\ -A(\varepsilon^{\max})\dfrac{\mathrm{d}}{\mathrm{d}r_i}\delta V(\varepsilon^{\max}) - \dfrac{dA(\varepsilon^{\max})}{dr_i}\displaystyle\sum_{j=1}^{N_b}\delta V(\varepsilon^{\max}), & \text{if } \varepsilon_i = \varepsilon^{\max} \end{cases} \quad (11)$$

To clarify how these equations work, consider two H_2, one with $\varepsilon_1 = 0.44$ and the other with $\varepsilon_2 = 0.45$ ($\varepsilon^{\max}$). Assume $q = 0.5$ and $\Delta V^{\max} = 30$ kcal/mol. Then, the boost force added to the first H_2 would be eq 11 case 1, which leads to a boost force of 22.89 kcal·mol^{-1}·Å^{-1}. However, the boost force added to the second H_2 would be case 2, 23.41 + 30.17, which leads to 53.58 kcal·mol^{-1}·Å^{-1}. The extra term (30.17) arises because the excess energy in the first H_2 flows into the reactive bond. This formulation provides an unequal treatment for small changes for a normal bond, but large changes in the most reactive bond.

A key issue in accelerated dynamics is how to convert accelerated time scale to physical time (hypertime). The original form of time reweighing is[8]

$$t_{\text{hyper}} = \sum_{i=1}^{N_{\text{tot}}}\Delta t_{\text{sim}}\exp(\Delta V^i/k_BT) \quad (12)$$

where N_{tot} is the number of integration steps, and Δt_{sim} is the time step of MD simulation. To achieve good statistics, the simulation should be sufficiently long to sample enough boost regions. This means that large numbers of transitions should be included to reduce the relative error.

Recently, Kim et al. proposed a modified reweighing method:[43]

$$t_{\text{hyper}} = \sum_{i=1}^{N_{\text{tot}}}\Delta t_{\text{sim}}\frac{\rho_{V_b}(r)}{\rho(r)}\exp(\Delta V^i/k_BT) \quad (13)$$

where $\rho(r)$ is the probability distribution of bond length in the original potential and $\rho_{V_b}(r)$ is the probability distribution in the biased simulation. The probability distributions of bond length can be obtained easily from separate short MD simulations. Once we have this information, the accuracy of reweighting can be improved, even when the transition times between reactions are short, which is often the case in simulating chemical reactions.

2.2. aARRDyn Parameters. For ReaxFF the r^{eq} parameters are the equilibrium bond lengths of the bonded atoms, which are 0.750 Å (H−H), 0.950 Å (O−H) and 1.250 Å (O−O). P_1 was introduced to adjust the stiffness of the boost potential at the boundary of the boosted region of phase space. If P_1 is small, ΔV increases more slowly at the boundary between the boosted and unboosted regions of phase space making it less likely to create a steep wall or peak.

Thus, the parameters in aARRDyn are (i) q, the maximum bond fluctuation to be considered for a BB, which we take as $q = 0.5$. (Note that this is not the BO limit; rather it is the maximum ratio of the current bond distance to the equilibrium r^{eq}. We use 0.5 here because the H−H bond is very short.) (ii) P_1, the bond boost stiffness, which we take as $P_1 = 0.98$ as the original BB paper.[13] (iii) $\Delta V^{\max}$, the bond boost that adjusts during the dynamics to control the boost amplitude.

2.3. Determining the Radicals. A problem inherent to rare-event simulation methods is that some reaction steps may already have small barriers that we do NOT want to accelerate. For hydrogen combustion, the small-barrier events are the radical recombination reactions, such as H + O → OH, H + OH → H_2O, and HO + HO → HOOH. These have very small barriers and do not need a bond boost. Thus, for aARRDyn we track how many radicals there are at every simulation step. Only when no radicals exist, is the boost turned on to accelerate the system. Otherwise, the boost is off.

A general approach to detect radicals was devised using the undercoordination and overcoordination terms from ReaxFF, which compares the calculated sum of bond orders (Sum(BO)) to an atom with the valence of the atom (e.g., 4 for C, 1 for H, and 2 for O). Thus, we consider an H atom to be an H radical, if the undercoordination number is −1, which means no bonds at all. Taking into account fluctuations in the dynamics, we consider that H is under coordinated (a radical) if $\text{BO}_{\text{sum}} < 0.3$, leading to undercoordination < −0.7.

For a molecule containing O atoms, we use both under-coordination and overcoordination to assess whether the molecule is a radical. Thus, both O atom and OH radical are under coordinated. But for HO_2, the bond order of the HO bond order is 1 while the bond order of the OO bond is 1.5, so that the central oxygen atom is over coordinated by 0.5 while the outer O is under-coordinated by

dx.doi.org/10.1021/ja5037258 | J. Am. Chem. Soc. 2014, 136, 9434−9442

−0.5. Thus, we consider an oxygen atom to be a radical, if either $BO_{sum} < 0.3$ or $BO_{sum} > 2.4$, which corresponds to under coordination ←0.7 or over coordination > +0.4. These under/over coordination numbers are already calculated at every step for ReaxFF.

2.4. Bond Boost in ReaxFF. The general procedure for performing aARRDyn using ReaxFF is as follows:

(1) Start with the new geometry predicted from a previous step of RMD and calculate forces using ReaxFF.

(2) Perform the radical analysis using ReaxFF under/over-coordination data. If the number radicals are less than 2, go to step 3 to perform bond boost acceleration; otherwise, (no bond boost) go to step 5.

(3) Tag each atom having a corrected bond order $BO_i \leq BO_{max} = 0.3$, Denote this number as N_{tag}.

(4) Determine ε^{max}. If $\varepsilon^{max} < q$ ($q = 0.5$), then calculate the boost force; otherwise, (no bond boost) go to step 5. Thus, we calculate a BB only when a particular bond has $BO > BO_{cut} = 0.3$ and simultaneously the extension of this bond beyond equilibrium is not more than 50%. For example, a bond with BO = 1 and $r = r^{eq}$ would be considered for a BB. Thus, the majority of bonds are considered for a BB. However, for bonds having a small ε, the extra energy is small. We then sum up these extra incremental energies for all the bonds considered for the BB, and focus this energy on the bonds with the higher ε. In this way only bonds near the threshold of ε get the most boost. Of course changing just the energy does not lead to a force that would modify the dynamics. This bond boost is converted into a force by eq 11.

(5) Use modified forces to predict changes in velocities and coordinates and go to step 1 for the next dynamics iteration.

2.5. Simulation Details. In carrying out these RMD simulations we found that the ReaxFF-COH2008 version of the ReaxFF force field was not accurate for such intermediates as H_3O. Consequently we reoptimized the fit to QM, leading to the ReaxFF-OH2014 force field that was used in the simulations. The parameters and validation of ReaxFF-OH2014 are reported in the Supporting Information.

The simulations of hydrogen combustion were carried out using the set of OH ReaxFF parameters (ReaxFF-OH2014), which are summarized in the Supporting Information. NVT MD simulations were performed with a time step of 0.25 fs, using the Nose-Hoover thermostat[44] to control temperature. The in-house revised version of PuReMD software was used in all simulations.[42]

The cubic simulation box was fixed at sides of 2.5 nm and initially contained 66 H_2 and 33 O_2 molecules. The H_2 and O_2 molecules were inserted into the box randomly using Packmol[45] and equilibrated with ReaxFF at 298 K for 100 ps at 298 K, which leads to a pressure of 260.56 atm.

We then heated the system to the target temperatures (798, 1098, 1498, 1898, 2298, 2498, 2698, and 2998 K) at a rate of 10 K/ps. This leads to initial pressures at these temperatures ranging from 673.23 to 2788.71 atm. We built 19 boxes independently to provide statistical analysis. For each of the simulation boxes, we carried out 2 to 20 ns of NVT simulations. At the end of the BF-RMD calculations, the final average pressures ranged from 450.23 to 862.45 atm.

3. RESULTS AND DISCUSSION

3.1. Combustion at 2498 K. We chose to compare the simulation results between BF-RMD and aARRDyn at a temperature of 2498 K. This is reasonable, given it lies between the ignition temperature (798 K) and the combustion temperature (2998 K) of hydrogen. More importantly the reaction rate at 2498 K is sufficiently fast that it only takes 10 ns for BF-RMD simulation to provide sufficient reaction data. The reaction rates and reaction mechanisms produced in BF-RMD serve as a reference for validating the accuracy of aARRDyn. We expect that aARRDyn should reproduce both the kinetics and the reaction mechanisms (within statistical errors).

In aARRDyn simulations, the only adjustable parameter is ΔV^{max}. Larger ΔV^{max} produces larger boost potentials, increasing the pace of the reactions. Thus, increased ΔV^{max} decreases computational time, but too large a ΔV^{max} might modify the kinetics. Thus, if the boost potential is too large, it could make the potential energy surface too flat, leading to a random walk among excited species, which would not reflect the true reaction kinetics. This might reduce the kinetic differences between favorable and unfavorable reaction steps that might allow unrealistic chemical reactions. Moreover, the calculation of hypertime depends exponentially on ΔV^{max} (eq 12 and 13)), so that too large a value might lead to uncertainties in assessing hypertime. A good boost potential should provide both efficiency and accuracy.

Our choices for ΔV^{max} were based on the bond energy. In ReaxFF the strength of the H−H bond is 108.72 kcal/mol while the strength of the O−O bond is 125.93 kcal/mol. Thus, we choose ΔV^{max} to be less than $^1/_2$ of these values or 54 kcal/mol. We considered three values, 20, 30, and 40 kcal/mol, all of which we consider to provide kinetics and mechanism the same as for BF-RMD. Figure 1 compares with BF-RMD the rate of water generation for these different values of ΔV^{max}. (We also extended our simulation to larger ΔV^{max}. The results are shown in Supporting Information, Figure S2). For aARRDyn, the simulation time is 0.5 ns for ΔV^{max} = 20 and 40 but 1.0 ns for ΔV^{max} = 30. For BF-RMD, we extended the simulation to 10 ns

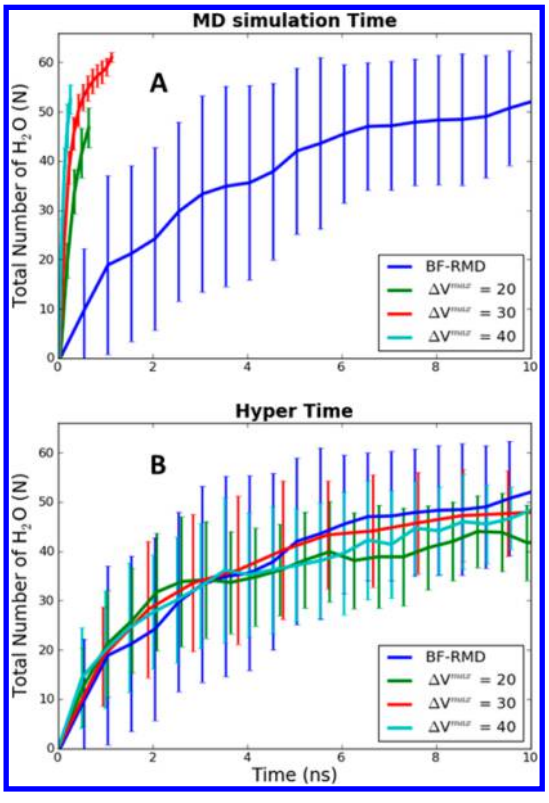

Figure 1. Comparison between BF-RMD and aARRDyn of H_2O products generated from combustion of H_2 at 2498 K as a function of (A) the MD simulation time and (B) hypertime. Here we considered ΔV^{max} = 20, 30, and 40 kcal/mol. For BF-RMD, the physical time is the simulation time. For aARRDyn, the physical time is converted to hypertime by reweighing the simulation time using eq 13 as shown in Table 1. The colors are as follows: BF-RMD, blue; aARRDyn, with ΔV^{max} =20 kcal/mol, green = 30 kcal/mol, red and = 40 kcal/mol cyan. The colors of the error bars are the same as the lines. The H_2 loss curve and H_2O_2 formation curve are shown in the Supporting Information (Figures S5 and S6).

dx.doi.org/10.1021/ja5037258 | J. Am. Chem. Soc. 2014, 136, 9434−9442

Table 1. Comparison of the Simulation Times (t_{sim}) and Hypertimes (t_{hyper}) for 50% H_2 Loss ($t_{reactant}$) and for Forming 50% of the H_2O Products ($t_{production}$) at 2498 K[a]

		$t_{reactant}$ (ns)		$t_{production}$ (ns)		
simulation	ΔV^{max}	t^{sim}	t^{hyper}	t^{sim}	t^{hyper}	boost factor
aARRDyn	40	0.13 (0.07)	4.01(2.37)	0.14(0.04)	4.28(3.42)	30.57
aARRDyn	30	0.18(0.06)	2.74(1.24)	0.20(0.06)	2.97(2.44)	14.85
aARRDyn	20	0.37(0.07)	3.62(2.74)	0.41(0.06)	3.88(3.90)	9.46
BF-RMD		3.30(2.19)	3.30(2.19)	3.51(2.32)	3.51(2.32)	1.0

[a]We consider the BF-RMD simulation along with three cases of aARRDyn, with ΔV^{max} = 20, 30, and 40 kcal/mol. All data in the Table are averaged from 19 independent simulations, with the uncertainties (in parentheses) estimated from this sampling. The boost factors (the ratio of hypertime and simulation time) are calculated based on $t_{production}$. The excellent agreement of the hypertime for both loss of reactant and for formation of the validates the aARRDyn methodology.

in order to observe sufficient reactions. In every case, the water generation curve is averaged from 19 independent simulations.

To obtain a quantitative reaction rate, we can compare the time to make $^1/_2$ the products, that is the time to form 33 water molecules. This is not a real reaction rate since a number of reaction processes are convoluted. Table 1 compares $t_{product}$ for both simulation time and hyper-time for aARRDyn and BF-RMD simulations. After reweighting to hyper-time, all simulations show similar $t_{product}$. Thus, for aARRDyn with ΔV^{max} = 40, 30 and 20, $t_{product}$ = 4.28 ± 3.42, 2.97 ± 2.44, and 3.88 ± 3.90 ns compared with 3.51 ± 2.32 ns for BF-RMD. Thus, within the error bars, all aARRDyn simulations converge to the BF-RMD simulation after time reweighting, which is one criterion for establishing that the kinetics in aARRDyn simulation are correct.

The efficiency of the BB simulations can be expressed as the ratio of hypertime and simulation time, the boost factor. For ΔV^{max} = 20, 30, and 40, the boost factors are 9.46, 14.85, and 30.57.

A second measure to compare is the rate of reactant disappearance. Here a useful metric is the half-life reaction time ($t_{reactant}$), which is the time for 50% of the fuel reactants to react, that is, for 33 H_2 to disappear. This is also compared in Table 1, where we see that $t_{reactant}$ is about 0.21 ns (210 ps) shorter than $t_{production}$ in all the cases. These 210 ps include also the time for the H_2O_2 formed during the early reaction times to finally convert to the final HOH product (~150 ps). In aARRDyn simulations, the H_2O_2 decomposition is also accelerated, taking 30, 15, and 10 ps in aARRDyn with ΔV^{max} = 20, 30 and 40, respectively. When converted to hypertime, the differences between $t_{reactant}$ and $t_{production}$ are 140 ps, 187 ps, and 205 ps, consistent with the BF-RMD simulation (150 ps) and within the corresponding statistical error (Table 1).

3.2. Reaction Mechanism. Of course the most important reason for atomistic level simulations of chemical reaction systems is to determine the reaction mechanism, that is, the sequence of steps and rates that convert reactants to products. To validate aARRDyn, we must determine how well it reproduces the reaction mechanism found with BF-RMD. Here we used ensemble-averaged trajectories to analyze the reaction mechanisms. To perform a complete comparison, we averaged all 19 simulations for BF-RMD simulations and compared the results with those obtained by aARRDyn simulations, starting with the same initial configuration and velocities.

Figure 2 shows the major species generated during the simulation, which include two stable products, H_2O and HOOH, and three active species HO_2, HO, and H. The production of O atoms was too small to be significant.

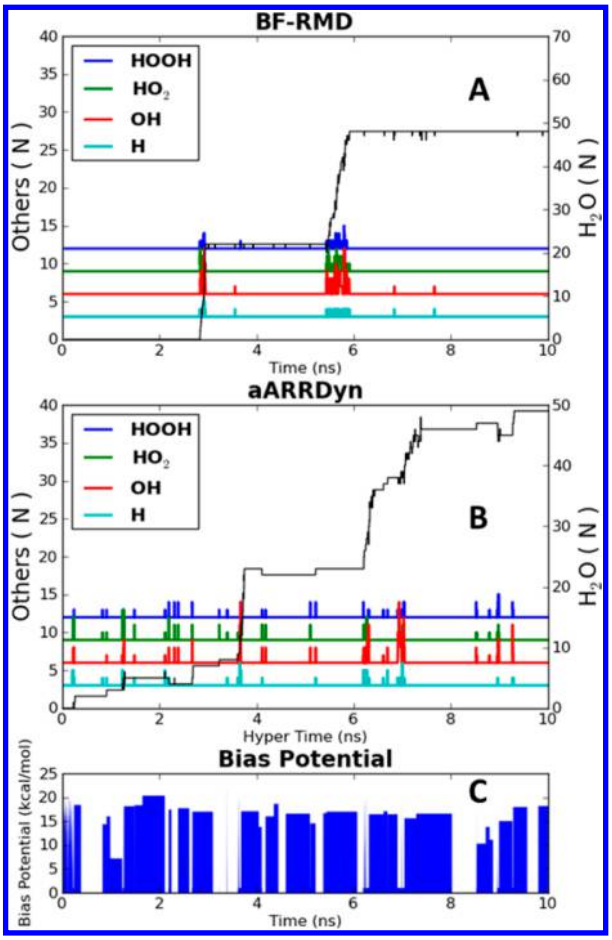

Figure 2. Comparison of the numbers of intermediate species generated by (A) BF-RMD and (B) aARRDyn simulations (ΔV^{max} = 30 kcal/mol) at 2498 K and (C) the corresponding bias potential. Both simulations were carried out starting from exactly the same initial configurations and velocities. The simulation times are 10 ns for BF-RMD and 1 ns for aARRDyn. The time shown for aARRDyn is the hypertime. The populations of H_2O are shown in the right *y*-axis; the others are shown in the left *y*-axis. For clarity, the data on H, OH, HO_2, and HOOH are shifted by 3, 6, 9, and 12, respectively. The production of O atoms was too small to show here. The bias potential along with the simulation time are shown in (C) for ΔV^{max} = 30 kcal/mol. The other two cases (ΔV^{max} = 20 and 40 kcal/mol) are in Supporting Information (Figures S7 and S8).

The first intermediate formed was HO_2 along with H. This came from the reaction

$$H_2 + O_2 \rightarrow H + HO_2 \quad (r1)$$

dx.doi.org/10.1021/ja5037258 | J. Am. Chem. Soc. 2014, 136, 9434−9442

Table 2. Analysis of the Reaction Frequencies for the Final Step of H_2O Production[a]

		aARRDyn (%)			
	reactions	40	30	20	BF-RMD (%)
r5	$H_2 + OH = H + H_2O$	62(6)	59(7)	60(9)	62(12)
r6	$H + OH = H_2O$	17(5)	19(6)	20(7)	16(8)
r7	$OH + HO_2 = H_2O + O_2$	9(3)	9(4)	5(4)	8(4)
r4	$H + HOOH = OH + H_2O$	4(3)	5(5)	6(5)	6(6)
r3	$H_2 + HO_2 = H_2O + OH$	4(2)	4(3)	4(3)	5(4)
r8	$H + HO_2 = H_2O + O$	3(4)	3(3)	4(3)	2(4)
r9	$HO_2 + HOOH = OH + H_2O + O_2$	1(3)	1(3)	1(3)	1(3)

[a]Listed here are the percentages of those reactions producing water molecules at 2498 K. The data are obtained from 19 independent simulations by BF-RMD and aARRDyn with ΔV^{max} =20, 30, and 40 kcal/mol. The root mean square (RMS) differences are shown in parentheses. The close correspondence between BF-RMD and the three aARRDyn cases validates the aARRDyn methodology.

Table 3. Analysis of the Reaction Frequencies for HOOH Generation and Loss during the Simulation[a]

		aARRDyn (%)			
	reactions	40	30	20	BF-RMD (%)
	HOOH Generation				
r3	$H_2 + HO_2 = HOOH + H$	42(11)	44(19)	43(12)	44(17)
r10	$H + HO_2 = HOOH$	29(13)	28(16)	39(16)	34(18)
r11	$HO_2 + HO_2 = HOOH + O_2$	23(9)	19(8)	14(11)	17(8)
r12	$OH + OH = HOOH$	5(9)	8(11)	3(8)	4(8)
r13	$H_2O + HO_2 = HOOH + OH$	1(13)	1(13)	1(12)	1(14)
	HOOH Loss				
r14	$HOOH = OH + OH$	68(19)	66(16)	67(17)	72(16)
r4	$H + HOOH = H_2O + OH$	31(6)	33(11)	32(11)	27(12)
r15	$HOOH + O = OH + HO_2$	1(6)	1(7)	1(6)	1(10)

[a]Listed here are the percentages of generation reactions that produce HOOH molecules and four HOOH loss reactions (at 2498 K). The data are obtained from 19 independent simulations by BF-RMD and aARRDyn with ΔV^{max} = 20, 30, and 40 kcal/mol. The RMS differences are shown in parentheses. The close correspondence between BF-RMD and the three aARRDyn cases validates the aARRDyn methodology.

in which either or both of the H_2 and O_2 had been energized from previous collisions. We find that this H radical reacts quickly with another O_2 to form a second HO_2,

$$H + O_2 \rightarrow HO_2 \quad \text{(r2)}$$

so that the combination of these two steps can be considered as $H_2 + 2O_2 \rightarrow 2HO_2$.

We find that HO_2 induces a sequence of radical reactions:

$$HO_2 + H_2 \rightarrow H + HOOH \quad \text{(r3)}$$

$$H + HOOH \rightarrow H_2O + OH \quad \text{(r4)}$$

$$H_2 + OH \rightarrow H + H_2O \quad \text{(r5)}$$

which continue to produce water and HOOH. After these reactive radicals are fully consumed by termination reactions (forming H_2O or HOOH), the system returns to a nonreactive period waiting for the next radical induction event. This is illustrated in Figure 2, which shows the actual bond boosts. When radicals appear, the boost is turned off (no signal in the figure). After the radicals are fully consumed, the boost is turned on again. In this case, ΔV^{max} = 30 kcal/mol, the maximum boost in the simulations was 22.31 kcal/mol. The average boost potential energy was 17.71 kcal/mol (averaging only the cases with nonzero boost).

We show in Table 2 all reactions generating water. Here reaction r5 is a radical propagation reaction, in which the radical (OH) reacts with a reactant (H_2) to produce a second radical (H) plus H_2O. We expect this to be fast and indeed reaction r5 accounts for 62% of H_2O generation. Reaction r6 is a radical termination reaction, and accounts for 16% of the H_2O generation.

$$H + OH \rightarrow H_2O \quad \text{(r6)}$$

The remaining reactions are as follows:

- r7, a radical termination reaction, accounts for 8% of H_2O production. This is

$$OH + HO_2 \rightarrow H_2O + O_2 \quad \text{(r7)}$$

- r4, a radical propagation reaction accounts for 6% of H_2O production
- r3, a radical propagation reaction, accounts for 5% of H_2O production
- r8 a radical propagation reaction accounts for 2% of H_2O production

$$H + HO_2 \rightarrow H_2O + O \quad \text{(r8)}$$

- r9 a radical termination reaction accounts for 1% of H_2O production,

$$HO_2 + HOOH \rightarrow OH + H_2O + O_2 \quad \text{(r9)}$$

dx.doi.org/10.1021/ja5037258 | J. Am. Chem. Soc. 2014, 136, 9434−9442

Thus, aARRDyn leads to the same reaction steps as BF-RMD and with the same percentages (within statistical fluctuations), indicating that aARRDyn captures the atomistic reaction mechanism.

Table 3 shows reactions related to the other stable product molecule, HOOH, in r3 and which forms during the combustion, but finally reacts to form water. Here we list both reactions related to the generation and to loss of HOOH.

The most important reactions generating HOOH are r3 and radical recombination r10:

$$H + HO_2 \rightarrow HOOH \quad \text{(r10)}$$

These two reactions account for 78% of the HOOH production. The remaining reactions are

- r11, a radical termination reaction, accounts for 17% of HOOH production:

$$HO_2 + HO_2 \rightarrow HOOH + O_2 \quad \text{(r11)}$$

- r12, also a radical termination reaction, accounts for 4% of HOOH production:

$$OH + OH \rightarrow HOOH \quad \text{(r12)}$$

- r13 a radical propagation reaction, accounts for 1% of HOOH production:

$$H_2O + HO_2 \rightarrow OH + HOOH \quad \text{(r13)}$$

The most important reactions for the subsequent destruction are r14 and r4, which account for 99%. In r14 the HOOH decomposes into 2OH radicals (energized by collisions with other molecules). When no radicals are present, this mechanism eventually occurs but it needs an induction time, which we find to be about 150 ps at 2498 K for BF-RMD. aARRDyn accelerates this reaction, requiring 30, 15, and 10 ps for ΔV^{max} = 20, 30, and 40 kcal/mol. Converted to hypertime, the induction times for r14 are 140, 187, and 205 ps, which are consistent with the BF-RMD values (150 ps). The remaining reaction r15 generates only trace amount of HOOH, accounting for 1% of the HOOH loss.

As shown in Table 3, aARRDyn reproduces well the relative ratios of both the generation and loss of HOOH. These results are in excellent agreement with the reaction distributions and serve to validate that aARRDyn reproduces the correct reaction mechanisms.

3.3. Kinetics over the Temperature Range from Ignition to Combustion. To explore the capabilities of the aARRDyn method to describe the lower temperature processes that are completely impractical with BF-RMD, we extended our simulation to the full temperature range of H_2 combustion, from ignition temperature (798 K) to flame temperature (2698 K). At low temperatures, BF-RMD is too slow to produce enough data for validation. Thus, for validating aARRDyn, we used the BF-RMD NVT simulations ranging from 2498 K to 2998 K to estimate the apparent activation energy and pre-exponential terms and then used these to predict the BF-RMD kinetics at lower temperatures. Figure 3 shows the results which lead to ΔH^{act} = 59.01 kcal/mol and $A = (kT/h)\exp(\Delta S^{act}/R)$ where ΔS^{act} = −4.97 J·K^{-1}·mol^{-1}. This ΔH^{act} is ∼$^1/_2$ the bond energy of the weakest bond (108.72 kcal/mol for H_2), which is consistent with the dominant process involving formation of an H_2−O_2 complex which is activated by collision of a third particle to form effectively two H radicals.

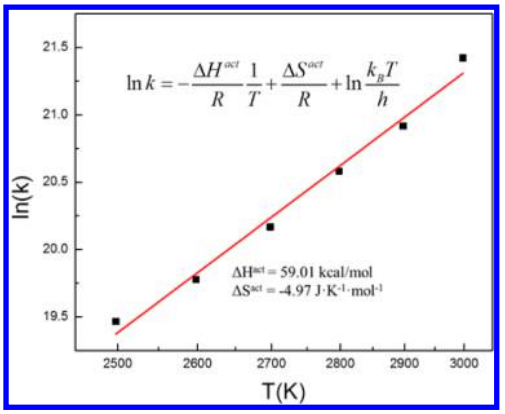

Figure 3. Arrhenius analysis for the overall rate constant of H_2O production derived from BF-RMD NVT simulations at 2498, 2598, 2698, 2798, 2898, and 2998 K. *X*-axis is in reciprocal scale. The solid line is the least-squares fit. The optimum kinetic parameter ΔH^{act} = 59.01 kcal/mol, which can be compared to half the ReaxFF bond enthalpy of H_2, at a high temperature of 109.56/2 + 2*R* = 58.74, suggesting that H_2 dissociation dominates the rate. The pre-exponential factor from transition state theory is $A = (k_B T/h)\exp(\Delta S^{act}/R)$ leading to ΔS^{act} = −4.55 J·K^{-1}·mol^{-1}. The entropy of H_2 and O_2 at 2000 K are 187.10 and 258.70 J·K^{-1}·mol^{-1}, and the entropy of H and HO_2 are 154.17 and 312.72 J·K^{-1}·mol^{-1} at 2498 K. This ΔS^{act} is consistent with the rate-determining step involving H_2 and O_2 forming a weakly bound cluster that is subsequently activated by a collision with another H_2 or O_2 to form an H atom and an HO_2. Then, the H reacts with O_2 to form another HO_2.

For aARRDyn simulations, we used boost potentials of ΔV^{max} = 20, 30, and 40 kcal/mol ranging from 798 K to 2698 K. The reaction kinetics ($t_{half\text{-}life}$ of production) at these three temperatures together with previous 2498 K data are shown in Figure 4 and Table 4.

On the basis of the kinetic parameters for BF-RMD, we find that the hypertimes for the aARRDyn simulations at 798 K

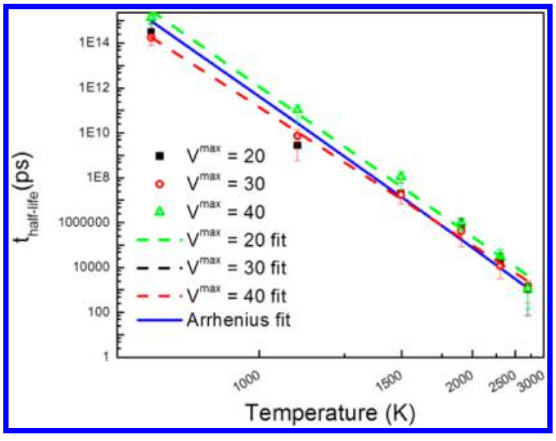

Figure 4. Half-time for product formation $t_{product}$ in hypertime for aARRDyn at temperatures from 798 K to 2698 K. This is compared with the Arrhenius fit (solid line) to BF-RMD at temperatures from 2498 to 2998 shown in Figure 3. Fitting the Arrhenius rate expression instead to the aARRDyn hypertimes over the full temperature range from 798 K to 2698 K leads to the dashed lines. The average of these three aARRDyn simulations leads to ΔH^{act} = 57.97 kcal/mol and ΔS^{act} = −13.557 J·K^{-1}·mol^{-1}. This more negative value of ΔS^{act} is consistent with formation of the H_2 plus O_2, which would be sampled more often at the lower temperatures. The *x*-axis uses reciprocal scaling, while a log scale is used for the *y*-axis.

dx.doi.org/10.1021/ja5037258 | J. Am. Chem. Soc. 2014, 136, 9434−9442

Table 4. Temperature Dependence (from 798 K to 2698 K) of the Simulation Times (ps) and Hypertime (ps) for Forming 50% of the H_2O Products for aARRDyn with ΔV^{max} = 20, 30, and 40 kcal/mol[a]

		H_2O (ps)		
temp (K)	ΔV^{max}	$t^{sim}_{half\text{-}life}$	$t^{hyper}_{half\text{-}life}$	boost factor
798	40	7.67×10^2	1.41×10^{15}	1.83×10^{12}
	30	1.25×10^3	1.77×10^{14}	1.41×10^{11}
	20	1.85×10^3	3.25×10^{14}	1.75×10^{11}
1098	(BF-RMD)		9.73×10^{14}	
	40	6.56×10^2	1.07×10^{11}	1.63×10^8
	30	7.71×10^2	7.42×10^9	0.96×10^7
	20	1.14×10^3	2.80×10^9	2.45×10^6
	(BF-RMD)		2.72×10^{10}	
1498	40	4.01×10^2	1.12×10^8	2.79×10^5
	30	4.70×10^2	1.79×10^7	3.80×10^4
	20	6.48×10^2	2.12×10^7	3.27×10^4
	(BF-RMD)		1.46×10^7	
1898	40	2.69×10^2	9.95×10^5	3.70×10^3
	30	2.99×10^2	4.38×10^5	1.46×10^3
	20	5.01×10^2	6.37×10^5	1.27×10^3
	(BF-RMD)		1.76×10^5	
2298	40	1.54×10^2	3.20×10^4	2.08×10^2
	30	2.31×10^2	1.22×10^4	0.53×10^2
	20	4.44×10^2	2.07×10^4	0.47×10^2
	(BF-RMD)		$9{,}57 \times 10^3$	
2698	40	1.13×10^2	1.15×10^3	10.18
	30	1.31×10^2	1.47×10^3	11.22
	20	2.46×10^2	1.07×10^3	4.33
	(BF-RMD)		1.20×10^3	

[a]This is compared with the BF-RMD results extrapolated from higher temperature BF-RMD (from Figure 3). All data in this Table are averaged from 19 independent simulations, with the uncertainties quoted in parentheses. The boost factors are calculated based on the ratio of hypertime and simulation time. The RMS differences are shown in parentheses. Note that the BF-RMD* denotes the extrapolated values.

range from 177 to 1410 s with an average of 538 s (5.38×10^{14} ps) at a computational cost from 767 to 1850 ps with average of 1289 ps. This shows the power of aARRDyn, leading to reasonable descriptions near ignition at 798 K with a boost factor of 0.42×10^{12}. Figure 4 shows the comparison of the $t_{half\text{-}life}$ time between aARRDyn for various BB and the theoretical value estimated from BF-RMD, where we find good agreement.

Fitting the rates from aARRDyn simulations over the full temperature range of 798 to 2698 K to $K = (k_B T/h) \exp(\Delta S^{act}/R) \exp(-\Delta H^{act}/RT)$, leads to ΔH = 56.40 kcal/mol and ΔS^{act} = -14.52 J·K^{-1}·mol^{-1} for ΔV^{max} = 20, ΔH = 56.30 kcal/mol and ΔS^{act} = -14.28 J·K^{-1}·mol^{-1} for ΔV^{max} = 30 and ΔH = 61.21 kcal/mol and ΔS^{act} = -11.874 J·K^{-1}·mol^{-1} for ΔV^{max} = 40. The average of three aARRDyn simulations is ΔH^{act} = 57.97 kcal/mol and ΔS^{act} = -13.557 J·K^{-1}·mol^{-1} which can be compared to ΔH^{act} = 59.01 kcal/mol and ΔS^{act} = -4.55 J·K^{-1}·mol^{-1} from BF-RMD done over the range of 2498 K to 2998 K. This more negative value of ΔS^{act} aARRDyn is consistent with formation of the H_2 plus O_2, which would be more stable at the lower temperatures. Thus, we consider that the aARRDyn results are more reliable, in which a larger temperature range can be explored.

We could not find experimental data for a direct comparison to our calculations. However, flow reactor experiments[46] for a $H_2/O_2/N_2$ mixture with H_2/O_2 = 0.3 and a total pressure or 6.5 atm at 884 K led to ΔH = 61.3 kcal/mol and ΔS = -32.14 J mol^{-1} K^{-1}.

4. CONCLUSION

This paper extends ReaxFF technology to address the remaining issue in first-principles-based simulations of reaction dynamics of complex systems by reducing the computational cost of such a long-term reaction process to a practical level.

Combining aARRDyn with ReaxFF provides the means for first-principles-based simulations to accurately describe the reaction rates and mechanism for large-scale complex reactions (assuming an accurate ReaxFF potential). Here, we demonstrated an example, showing that aARRDyn leads to the correct reaction kinetics of H_2 combustion while reducing the cost at the reaction initiation temperature by a factor of a trillion compared to BF-RMD. We found that the adaptive boost potential in aARRDyn did not alter the underlying reaction mechanisms, and we found that the hypertime estimation (acceleration) is accurate against BF-RMD. We expect that the kinetics parameters developed here, including the percentages for the steps of H_2 and HOOH loss and formation that provide relative rates, may be used to analyze the results of shock tube and combustion studies of hydrogen oxidation.

We expect that the aARRDyn methodology may be particularly valuable for describing biological processes where the temperatures must be <100 °C and the kinetics time scales may be microseconds and longer.

One might find a way to accelerate QM-based RMD to address some of these problems on small systems (up to a few hundred atoms). However, aARRDyn makes direct use of concepts like bond order, overcoordination, and undercoordination that are not defined in QM. Thus, aARRDyn provides a unique solution to this problem, while enabling significantly larger system length and time scales, and retaining the underlying physical insight.

■ ASSOCIATED CONTENT

Supporting Information

H_2O generation curves of all 19 samples, H_2O generation curves of ΔV^{max} = 50, 60, 70 and 80, potential energy and force curves, H_2 loss curve at 2498 K, H_2O_2 generation curve at 2498 K, species generated in aARRDyn simulations with ΔV^{max} = 20 and 40 kcal at 2498 K; the new ReaxFF-OH2014 force field parameters plus some of the validations against QM; results for the Arrhenius analysis, reaction mechanisms and kinetics from the older ReaxFF-CHO2008 force field, the force field file, and the plot script. This material is available free of charge via the Internet at http://pubs.acs.org.

■ AUTHOR INFORMATION

Corresponding Authors

ajaramil@caltech.edu
wag@wag.caltech.edu
huaisun@sjtu.edu.cn

Notes

The authors declare no competing financial interest.

■ ACKNOWLEDGMENTS

We thank Hai Xiao, Dr. Qi An and Wei-Guang Liu for insightful discussions. This work was funded by the Office of Naval Research (ONR N0014-12-1-0538), the US Department of Transportation, Federal Highway Administration (FHWA), (Award Number BAA No. DTFH61-09-R-00017), the Defense Advanced Research Projects Agency (DARPA N660011214037 and DARPA HR0011-14-2-0003), NSF CHE-1214158, and the National Science Foundation of China (Nos. 21073119 and 21173146), and the National Science Council of Taiwan, R.O.C (NSC 103-3113-P-008-001).

■ REFERENCES

(1) Dykstra, C. E. *Theory and Applications of Computational Chemistry: The First Forty Years*; Elsevier: Amsterdam, The Netherlands, 2005.
(2) Schlitter, J.; Engels, M.; Krüger, P.; Jacoby, E.; Wollmer, A. *Mol. Simul.* **1993**, *10*, 291.
(3) Dellago, C.; Bolhuis, P. G.; Geissler, P. L. In *Advances in Chemical Physics*; John Wiley & Sons, Inc.: New York, 2003; p 1.
(4) Amadei, A.; Linssen, A. B. M.; Berendsen, H. J. C. *Proteins: Struct., Funct., Bioinf.* **1993**, *17*, 412.
(5) Voter, A. F. *Phys. Rev. B* **1998**, *57*, R13985.
(6) Sugita, Y.; Okamoto, Y. *Chem. Phys. Lett.* **1999**, *314*, 141.
(7) Laio, A.; Parrinello, M. *Proc. Natl. Acad. Sci. U.S.A.* **2002**, *99*, 12562.
(8) Voter, A. F. *Phys. Rev. Lett.* **1997**, *78*, 3908.
(9) Kim, S. Y.; Perez, D.; Voter, A. F. *J. Chem. Phys.* **2013**, *139*, 144110.
(10) Sorensen, M. R.; Voter, A. F. *J. Chem. Phys.* **2000**, *112*, 9599.
(11) Shim, Y.; Borovikov, V.; Uberuaga, B. P.; Voter, A. F.; Amar, J. G. *Phys. Rev. Lett.* **2008**, *101*, 116101.
(12) Lu, C.-Y.; Makarov, D. E.; Henkelman, G. *J. Chem. Phys.* **2010**, *133*, 201101.
(13) Miron, R. A.; Fichthorn, K. A. *J. Chem. Phys.* **2003**, *119*, 6210.
(14) Miron, R. A.; Fichthorn, K. A. *Phys. Rev. Lett.* **2004**, *93*, 128301.
(15) Miron, R. A.; Fichthorn, K. A. *Phys. Rev. B* **2005**, *72*, 035415.
(16) Becker, K. E.; Fichthorn, K. A. *J. Chem. Phys.* **2006**, *125*, 184706.
(17) McLaughlin, K.; Fichthorn, K. *Bull. Am. Phys. Soc.* **2006**.
(18) Mignogna, M. H.; Fichthorn, K. A.; Hammerschmidt, T.; Kratzer, P.; Scheffler, M. *2006 AIChE Ann. Conf. Proc.* **2006**.
(19) Fichthorn, K.; Miron, R. In *Computer Simulation Studies in Condensed-Matter Physics XIX*; Springer: Berlin Heidelberg, 2009; p 7.
(20) Fichthorn, K. A.; Miron, R. A.; Wang, Y.; Tiwary, Y. *J. Phys.: Condens. Matter* **2009**, *21*, 084212.
(21) Hamelberg, D.; Mongan, J.; McCammon, J. A. *J. Chem. Phys.* **2004**, *120*, 11919.
(22) Hamelberg, D.; Shen, T.; McCammon, J. A. *J. Chem. Phys.* **2005**, *122*, 241103.
(23) de Oliveira, C. A. F.; Hamelberg, D.; McCammon, J. A. *J. Phys. Chem. B* **2006**, *110*, 22695.
(24) de Oliveira, C. A.; Hamelberg, D.; McCammon, A. *J. Chem. Phys.* **2007**, *127*, 175105.
(25) Hamelberg, D.; de Oliveria; McCammon, A. *J. Chem. Phys.* **2007**, *127*, 155102.
(26) Markwick, P. R. L.; Bouvignies, G.; Blackledge, M. *J. Am. Chem. Soc.* **2007**, *129*, 4724.
(27) Minh, D. D. L.; Hamelberg, D.; McCammon, J. A. *J. Chem. Phys.* **2007**, *127*, 154105.
(28) de Oliveira, C. A. F.; Hamelberg, D.; McCammon, J. A. *J. Chem. Theory Comput.* **2008**, *4*, 1516.
(29) Fajer, M.; Hamelberg, D.; McCammon, A. *J. Chem. Theory Comput.* **2008**, *4*, 1565.
(30) Shen, T.; Hamelberg, D. *J. Chem. Phys.* **2008**, *129*, 034103.
(31) Bucher, D.; Pierce, L. C. T.; McCammon, J. A.; Markwick, P. R. L. *J. Chem. Theory Comput.* **2011**, *7*, 890.
(32) Doshi, U.; Hamelberg, D. *J. Chem. Theory Comput.* **2011**, *7*, 575.
(33) Markwick, P. R. L.; Pierce, L. C. T.; Goodin, D. B.; McCammon, J. A. *J. Phys. Chem. Lett.* **2011**, *2*, 158.
(34) Pierce, L. C. T.; Markwick, P. R. L.; McCammon, J. A.; Doltsinis, N. L. *J. Chem. Phys.* **2011**, *134*, 174107.
(35) Sinko, W.; de Oliveira, C. A. F.; Pierce, L. C. T.; McCammon, J. A. *J. Chem. Theory Comput.* **2011**, *8*, 17.
(36) Doshi, U.; McGowan, L. C.; Ladani, S. T.; Hamelberg, D. *Proc. Natl. Acad. Sci. U.S.A.* **2012**, *109*, 5699.
(37) Trimm, D. L.; Önsan, Z. I. *Catal. Rev.* **2001**, *43*, 31.
(38) van Duin, A. C. T.; Dasgupta, S.; Lorant, F.; Goddard, W. A. *J. Phys. Chem. A* **2001**, *105*, 9396.
(39) Chenoweth, K.; van Duin, A. C. T.; Goddard, W. A. *J. Phys. Chem. A* **2008**, *112*, 1040.
(40) Agrawalla, S.; van Duin, A. C. T. *J. Phys. Chem. A* **2011**, *115*, 960.
(41) Chenoweth, K.; Cheung, S.; van Duin, A. C. T.; Goddard, W. A.; Kober, E. M. *J. Am. Chem. Soc.* **2005**, *127*, 7192.
(42) Aktulga, H. M.; Pandit, S. A.; Duin, A. C. T. v.; Grama, A. Y. *SIAM J. Sci. Comput.* **2012**, *34*, C1.
(43) Kim, W. K.; Falk, M. L. *J. Chem. Phys.* **2014**, *140*, 044107.
(44) Evans, D. J.; Holian, B. L. *J. Chem. Phys.* **1985**, *83*, 4069.
(45) Martínez, L.; Andrade, R.; Birgin, E. G.; Martínez, J. M. *J. Comput. Chem.* **2009**, *30*, 2157.
(46) Mueller, M. A.; Kim, T. J.; Yetter, R. A.; Dryer, F. L. *Int. J. Chem. Kinetics* **1999**, *31*, 113.